Available online at www.sciencedirect.com
ScienceDirect
International Journal of Heat and Mass Transfer 51 (2008) 111–124
International Journal of HEAT and MASS TRANSFER
www.elsevier.com/locate/ijhmt

New prediction methods for CO_2 evaporation inside tubes: Part I – A two-phase flow pattern map and a flow pattern based phenomenological model for two-phase flow frictional pressure drops

Lixin Cheng [a], Gherhardt Ribatski [a,b], Jesús Moreno Quibén [a], John R. Thome [a,*]

[a] *Laboratory of Heat and Mass Transfer (LTCM), Faculty of Engineering (STI), École Polytechnique Fédérale de Lausanne (EPFL), Station 9, Lausanne CH-1015, Switzerland*

[b] *Department of Mechanical Engineering, Escola de Engenharia de São Carlos (EESC), University of São Paulo (USP), São Carlos, SP 13566-590, Brazil*

Received 10 October 2006
Available online 7 June 2007

Abstract

An updated flow pattern map was developed for CO_2 on the basis of the previous Cheng–Ribatski–Wojtan–Thome CO_2 flow pattern map [1,2] to extend the flow pattern map to a wider range of conditions. A new annular flow to dryout transition (A–D) and a new dryout to mist flow transition (D–M) were proposed here. In addition, a bubbly flow region which generally occurs at high mass velocities and low vapor qualities was added to the updated flow pattern map. The updated flow pattern map is applicable to a much wider range of conditions: tube diameters from 0.6 to 10 mm, mass velocities from 50 to 1500 $kg/m^2 s$, heat fluxes from 1.8 to 46 kW/m^2 and saturation temperatures from −28 to +25 °C (reduced pressures from 0.21 to 0.87). The updated flow pattern map was compared to independent experimental data of flow patterns for CO_2 in the literature and it predicts the flow patterns well. Then, a database of CO_2 two-phase flow pressure drop results from the literature was set up and the database was compared to the leading empirical pressure drop models: the correlations by Chisholm [3], Friedel [4], Grönnerud [5] and Müller-Steinhagen and Heck [6], a modified Chisholm correlation by Yoon et al. [7] and the flow pattern based model of Moreno Quibén and Thome [8–10]. None of these models was able to predict the CO_2 pressure drop data well. Therefore, a new flow pattern based phenomenological model of two-phase flow frictional pressure drop for CO_2 was developed by modifying the model of Moreno Quibén and Thome using the updated flow pattern map in this study and it predicts the CO_2 pressure drop database quite well overall.
© 2007 Elsevier Ltd. All rights reserved.

Keywords: Model; Flow pattern map; Flow patterns; Phenomenological; Flow boiling; Two-phase flow; Frictional pressure drop; Macro-channel; Micro-channel; CO_2

1. Introduction

Carbon dioxide has been receiving renewed and intensive interest as an efficient and environmentally safe refrigerant in a number of applications, including mobile air conditioning, residential heat pump and hot water heat pump systems in recent years. Compared to other conventional refrigerants, the two-phase flow characteristics of CO_2, such as flow pattern, two-phase pressure drop and flow boiling heat transfer, are quite different from those of conventional refrigerants [1,2,11]. In order to design evaporators for these systems effectively, it is important to understand and predict the two-phase flow characteristics of CO_2 evaporation inside horizontal tubes. In the present study, a two-phase flow pattern map specifically for CO_2 and a flow pattern based phenomenological two-phase flow frictional pressure drop model are presented in Part I, and an updated flow pattern based flow boiling heat transfer model is presented in Part II.

* Corresponding author. Tel.: +41 21 693 5981; fax: +41 21 693 5960.
E-mail addresses: lixincheng@hotmail.com (L. Cheng), ribatski@sc.usp.br (G. Ribatski), jesus.moreno@epfl.ch (J. Moreno Quibén), john.thome@epfl.ch (J.R. Thome).

0017-9310/$ - see front matter © 2007 Elsevier Ltd. All rights reserved.
doi:10.1016/j.ijheatmasstransfer.2007.04.002

Nomenclature

A	cross-sectional area of flow channel, m^2
A_L	cross-sectional area occupied by liquid-phase, m^2
A_{LD}	dimensionless cross-sectional area occupied by liquid-phase
A_V	cross-sectional area occupied by vapor-phase, m^2
A_{VD}	dimensionless cross-sectional area occupied by vapor phase
D	internal tube diameter, m
Fr_L	liquid Froude number $[G^2/(\rho_L^2 g D_{eq})]$
$Fr_{V,Mori}$	vapor Froude number $[G^2/(\rho_v(\rho_L-\rho_v)gD_{eq})]$ defined by Mori et al. [42]
f	friction factor
G	total vapor and liquid two-phase mass flux, kg/m^2 s
g	gravitational acceleration, 9.81 m/s^2
h_L	vertical height of liquid, m
h_{LD}	dimensionless vertical height of liquid
h_{LV}	latent heat of vaporization, J/kg
L	tube length, m
N	number of data points
P_i	perimeter of interface, m
P_{iD}	dimensionless perimeter of interface
P_L	perimeter of tube wetted by liquid, m
P_{LD}	dimensionless perimeter of tube wetted by liquid
P_V	perimeter of tube in contact with vapor, m
P_{VD}	dimensionless perimeter of tube in contact with vapor
p	pressure, bar
p_r	reduced pressure $[p/p_{crit}]$
q	heat flux, W/m^2
Re_{LO}	Reynolds number considering the total vapor–liquid flow as liquid flow $[GD_{eq}/(\mu_L)]$
Re_M	Reynolds number $[GD_{eq}/(\mu_H)]$ defined in mist flow
Re_V	vapor phase Reynolds number $[GxD_{eq}/(\mu_V\varepsilon)]$
T_{sat}	saturation temperature, °C
u	mean average velocity, m/s
We_L	liquid Weber number $[G^2D_{eq}/(\rho_L\sigma)]$ defined by Eq. (16); $[\rho_L u_L^2 D_{eq}/\sigma]$ defined by Eq. (33)
We_V	vapor Weber number $[G^2D_{eq}/(\rho_v\sigma)]$ defined by Eq. (21)
x	vapor quality

Greek symbols

Δp	pressure drop, Pa
ε	cross-sectional vapor void fraction
ε_{IA}	vapor void fraction at $x = x_{IA}$
μ	dynamic viscosity, N s/m^2
θ_{dry}	dry angle of tube perimeter, rad
θ^*_{dry}	dimensionless dry angle $[\theta_{dry}/(2\pi)]$
θ_{strat}	stratified flow angle of tube perimeter, rad
θ^*_{strat}	dimensionless stratified flow angle $[\theta_{strat}/(2\pi)]$
θ_{wet}	wet angle of the tube perimeter, rad
ρ	density, kg/m^3
σ	surface tension, N/m; standard deviation, %
ξ_i	relative error, %
$\bar{\xi}$	average error, %
$\lvert\bar{\xi}\rvert$	mean error, %

Subscripts

A	annular flow
B	bubbly flow
crit	critical
de	dryout completion
di	dryout inception
dry	dry
dryout	dryout region
eq	equivalent
f	frictional
H	homogeneous
h	hydraulic
I	intermittent flow
IA	intermittent flow to annular flow transition
i	liquid–vapor interface, data point number
iD	interface in cross-section
in	tube inlet
L	liquid
LD	liquid in cross-section of the tube
LO	considering the total vapor–liquid flow as liquid flow
LV	liquid–vapor
M	mist flow
m	momentum; mean
out	tube outlet
Slug	slug flow
SW	stratified-wavy flow
static	static
strat	stratified flow
strat ($x \geqslant x_{IA}$)	stratified flow at $x \geqslant x_{IA}$
strat ($x < x_{IA}$)	stratified flow at $x < x_{IA}$
tp	two-phase flow
V	vapor
VD	vapor in cross-section of the tube
wavy	wavy flow
wet	wet perimeter

Flow patterns are very important in understanding the very complex two-phase flow phenomena and heat transfer trends in flow boiling. To predict the local flow patterns in a channel, a flow pattern map is used. In fact, successful flow pattern based flow boiling heat transfer and two-phase flow pressure drop models [8–10,12–14] have been

proposed in recent years. Over the past decades, many flow pattern maps have been developed to predict two-phase flow patterns in horizontal tubes, such as those by Baker [15], Taitel and Dukler [16], Hashizume [17], Steiner [18] and so on, just to name a few. Most were developed for adiabatic conditions and then extrapolated by users to diabatic conditions, thereby creating big discrepancies. For this reason, a number of diabatic flow pattern maps related to the corresponding heat transfer mechanisms have been developed [12–14,19,20]. However, none of these is applicable to CO_2 evaporation in horizontal tubes because the two-phase flow characteristics of CO_2 evaporation are greatly affected by the very high reduced pressures in many applications and low surface tensions of CO_2 [1,2,11]. In addition, the very low viscosities of CO_2 at high reduced pressures may affect the pressure drop greatly.

To fill in this void, a new CO_2 flow pattern map (the Cheng–Ribatski–Wojtan–Thome CO_2 flow pattern map) was recently developed in the Laboratory of Heat and Mass Transfer (LTCM) at the Swiss Federal Institute of Technology (EPFL) [1,2]. This flow pattern map is applicable to a wide range of test conditions for CO_2: tube diameters from 0.8 to 10 mm, mass velocities from 80 to 570 kg/m^2 s, heat fluxes from 5 to 32 kW/m^2 and saturation temperatures from −28 to +25 °C (reduced pressures from 0.21 to 0.87). However, this flow pattern map is not validated for the large mass velocities of industrial interest, which can reach 1500 kg/m^2 s in automobile air-conditioning systems. Therefore, a CO_2 flow pattern map covering a wider range of parametric conditions is needed to accurately predict the flow patterns for CO_2 evaporation and pressure drops in horizontal tubes.

As the predictions of two-phase flow frictional pressure drops with the leading methods often cause errors of more than 50% [8–10,21], efforts are increasingly being made to improve the accuracy of two-phase flow pressure drop predictions. In addition, the leading pressure drop prediction methods do not usually contain any flow pattern information, which is intrinsically related to the two-phase frictional pressure drop. As for CO_2, the leading prediction methods do not work well. The reason is that these methods do not usually cover the much lower liquid-to-vapor density ratios and very small surface tensions characteristic of CO_2 at high pressures. Due to these characteristics, normally the two-phase flow pressure drops of CO_2 are much lower than those of other refrigerants [1,2,11]. Significantly there is no proven, generally applicable two-phase pressure drop prediction method for CO_2, although there are a number of studies of CO_2 pressure drops in the literature [7,22–36]. Some researchers proposed pressure drop correlations for CO_2 based on their own experimental data but such methods cannot be extrapolated to other conditions. For example, Yoon et al. [7] proposed a modified Chisholm method to fit their data in a macro-scale channel but it cannot be applied to other conditions because there is only one diameter and a limited range of test conditions involved.

As opposed to the completely empirical two-phase pressure drop models, a flow pattern based phenomenological model relating the flow patterns to the corresponding two-phase flow pressure drops is a promising method in the two-phase pressure drop predictions. Ould-Didi et al. [21] used local flow patterns to analyze two-phase flow pressure drops, which resulted in a significant improvement in accuracy. Based on that, a new flow pattern based phenomenological model of two-phase frictional pressure drops was recently developed by Moreno Quibén and Thome [8–10]. The model physically respects the two-phase flow structure of the various flow patterns while maintaining a degree of simplicity as well. The model predicts their experimental data well but needs to be modified to predict the present CO_2 experimental database put together here.

In Part I of the present study, first, an updated general flow pattern map for CO_2, was developed to meet wider parametric conditions. The updated flow pattern map was compared to the recent flow pattern observations by Gasche [37]. Then, a large database of CO_2 two-phase flow pressure drop was set up and compared to the leading two-phase frictional pressure drop models: the correlations by Chisholm [3], Friedel [4], Grönnerud [5], Müller-Steinhagen and Heck [6], a modified Chisholm correlation by Yoon et al. [7] and the flow pattern based model of Moreno Quibén and Thome [8–10]. Finally, based on the updated CO_2 flow pattern map, an improved flow pattern based phenomenological model of two-phase flow frictional pressure drop was developed for CO_2, which is physically related to the flow patterns defined by the updated CO_2 flow pattern map.

2. Updated CO_2 flow pattern map

First, an updated CO_2 flow pattern map was developed based on the Cheng–Ribatski–Wojtan–Thome CO_2 flow pattern map [1,2] according to sharp changes of trends in flow boiling data that indicate such things as onset of dryout and onset of mist flow. In the present study, the physical properties of CO_2 have been obtained from REFPROP of NIST [38].

2.1. Updated flow pattern map for CO_2

For non-circular channels, equivalent diameters rather than hydraulic diameters were used in the flow pattern map, as

$$D_{eq} = \sqrt{\frac{4A}{\pi}} \tag{1}$$

Using the equivalent diameter gives the same mass velocity as in the non-circular channel and thus correctly reflects the mean liquid and vapor velocities, something using hydraulic diameter in a two-phase flow does not. In the updated CO_2 flow pattern map, several new features were developed

as compared to the Cheng–Ribatski–Wojtan–Thome flow pattern map [1,2]:

1. Combining with the updated flow boiling heat transfer model for CO_2 in Part II, the annular flow to dryout region (A–D) transition boundary was further modified so as to better fit the flow boiling heat transfer characteristics for higher mass velocities;
2. Based on experimental heat transfer data, a new criterion for the dryout region to mist flow (D–M) transition was proposed;
3. Bubbly flow occurs at very high mass velocities and very low vapor qualities, bubbly flow pattern boundary was integrated into the map to make it more complete.

With these modifications, the updated flow pattern map for CO_2 is now applicable to much higher mass velocities. Complete flow pattern transition criteria of the updated flow pattern map for CO_2 are described below.

As shown in Fig. 1, the six dimensionless geometrical parameters used in the flow pattern map are defined as [12–14]:

$$h_{LD} = \frac{h_L}{D_{eq}} \tag{2}$$

$$P_{LD} = \frac{P_L}{D_{eq}} \tag{3}$$

$$P_{VD} = \frac{P_V}{D_{eq}} \tag{4}$$

$$P_{iD} = \frac{P_i}{D_{eq}} \tag{5}$$

$$A_{LD} = \frac{A_L}{D_{eq}^2} \tag{6}$$

$$A_{VD} = \frac{A_V}{D_{eq}^2} \tag{7}$$

where D_{eq} is the internal tube equivalent diameter (for non-circular channels, equivalent diameter D_{eq} is used, for circular channels, equivalent diameter D_{eq} equals hydraulic diameter D_h, to make it clear, D_{eq} is used in this paper.), P_L is the wetted perimeter, P_V is the dry perimeter in contact with vapor, A_L and A_V are the corresponding cross-sectional areas of the liquid and vapor phases, P_i is the length of the phase interface and h_L is the height of the liquid phase from the bottom of the tube.

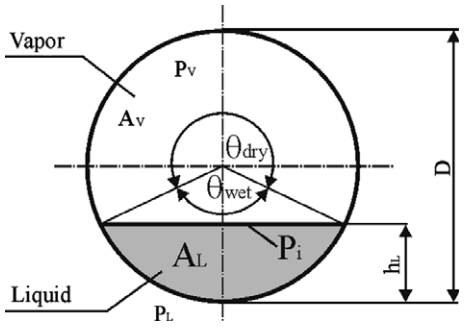

Fig. 1. Schematic diagram of stratified two-phase flow in a horizontal channel.

As a practical option and for consistency between the flow pattern map and the flow boiling heat transfer model, an easier to implement version of the flow map was proposed by Thome and El Hajal [39]. The void fraction ε which is determined with the Rouhani–Axelsson drift flux model [40] by Thome and El Hajal is kept the same in the present new flow map for CO_2 as

$$\varepsilon = \frac{x}{\rho_V}\left[(1+0.12(1-x))\left(\frac{x}{\rho_V}+\frac{1-x}{\rho_L}\right) + \frac{1.18(1-x)[g\sigma(\rho_L-\rho_V)]^{1/4}}{G\rho_L^{1/2}}\right]^{-1} \tag{8}$$

Then, the dimensionless parameters are determined as follows:

$$A_{LD} = \frac{A(1-\varepsilon)}{D_{eq}^2} \tag{9}$$

$$A_{VD} = \frac{A\varepsilon}{D_{eq}^2} \tag{10}$$

$$h_{LD} = 0.5\left(1-\cos\left(\frac{2\pi-\theta_{strat}}{2}\right)\right) \tag{11}$$

$$P_{iD} = \sin\left(\frac{2\pi-\theta_{strat}}{2}\right) \tag{12}$$

where the stratified angle θ_{strat} (which is the same as θ_{dry} shown in Fig. 1) is calculated with the equation proposed by Biberg [41]:

$$\theta_{strat} = 2\pi - 2\left\{\pi(1-\varepsilon)+\left(\frac{3\pi}{2}\right)^{1/3}[1-2(1-\varepsilon)+(1-\varepsilon)^{1/3}-\varepsilon^{1/3}] - \frac{1}{200}(1-\varepsilon)\varepsilon[1-2(1-\varepsilon)][1+4(1-\varepsilon)^2+\varepsilon^2]\right\} \tag{13}$$

Taking into account the modifications in the annular flow to dryout (A–D), dryout to mist flow (D–M) and intermittent flow to bubbly flow (I–B) transition curves which were newly developed in this study, the implementation procedure of the updated flow pattern map for CO_2 is as follows:

The void fraction ε and dimensionless geometrical parameters A_{LD}, A_{VD}, h_{LD} and P_{iD} are calculated with Eqs. (8)–(12). The stratified-wavy to intermittent and annular flow (SW–I/A) transition boundary is calculated with the Kattan–Thome–Favrat criterion [12–14]:

$$G_{wavy} = \left\{\frac{16A_{VD}^3 g D_{eq}\rho_L\rho_V}{x^2\pi^2[1-(2h_{LD}-1)^2]^{1/2}}\left[\frac{\pi^2}{25h_{LD}^2}\left(\frac{Fr_L}{We_L}\right)+1\right]\right\}^{1/2}+50 \tag{14}$$

where the liquid Froude number Fr_L and the liquid Weber number We_L are defined as

$$Fr_L = \frac{G^2}{\rho_L^2 g D_{eq}} \tag{15}$$

$$We_L = \frac{G^2 D_{eq}}{\rho_L \sigma} \tag{16}$$

Then, the stratified-wavy flow region is subdivided into three zones according the criteria by Wojtan et al. [19,20]:

- $G > G_{wavy}(x_{IA})$ gives the slug zone;
- $G_{strat} < G < G_{wavy}(x_{IA})$ and $x < x_{IA}$ give the slug/stratified-wavy zone;
- $x \geqslant x_{IA}$ gives the stratified-wavy zone.

The stratified to stratified-wavy flow (S–SW) transition boundary is calculated with the Kattan–Thome–Favrat criterion [12–14]:

$$G_{strat} = \left[\frac{226.3^2 A_{LD} A_{VD}^2 \rho_V (\rho_L - \rho_V) \mu_L g}{x^2 (1-x) \pi^3}\right]^{1/3} \tag{17}$$

For the new flow pattern map: $G_{strat} = G_{strat}(x_{IA})$ at $x < x_{IA}$.

The intermittent to annular flow (I–A) transition boundary is calculated with the Cheng–Ribatski–Wojtan–Thome criterion [1,2]:

$$x_{IA} = \left[1.8^{1/0.875}\left(\frac{\rho_V}{\rho_L}\right)^{-1/1.75}\left(\frac{\mu_L}{\mu_V}\right)^{-1/7} + 1\right]^{-1} \tag{18}$$

Then, the transition boundary is extended down to its intersection with G_{strat}.

The annular flow to dryout region (A–D) transition boundary is calculated with the new modified criterion of Wojtan et al. [19] based of the dryout data of CO_2 in this study:

$$G_{dryout} = \left\{\frac{1}{0.236}\left[\ln\left(\frac{0.58}{x}\right) + 0.52\right]\left(\frac{D_{eq}}{\rho_V \sigma}\right)^{-0.17} \left[\frac{1}{g D_{eq} \rho_V (\rho_L - \rho_V)}\right]^{-0.17}\left(\frac{\rho_V}{\rho_L}\right)^{-0.25}\left(\frac{q}{q_{crit}}\right)^{-0.27}\right\}^{1.471} \tag{19}$$

which is extracted from the new dryout inception equation in this study:

$$x_{di} = 0.58 e^{\left[0.52 - 0.236 We_V^{0.17} Fr_{V,Mori}^{0.17} (\rho_V/\rho_L)^{0.25} (q/q_{crit})^{0.27}\right]} \tag{20}$$

This equation remains the same as in the Wojtan et al. [19] flow map for low pressure refrigerants, except that new empirical parameters were obtained based on the CO_2 data since the previous expression did not extrapolate well to reduced pressures far higher than its underlying database. The vapor Weber number We_V and the vapor Froude number $Fr_{V,Mori}$ defined by Mori et al. [42] are calculated as

$$We_V = \frac{G^2 D_{eq}}{\rho_V \sigma} \tag{21}$$

$$Fr_{V,Mori} = \frac{G^2}{\rho_V (\rho_L - \rho_V) g D_{eq}} \tag{22}$$

and the critical heat flux q_{crit} is calculated with the Kutateladze [43] correlation as

$$q_{crit} = 0.131 \rho_V^{0.5} h_{LV} [g\sigma(\rho_L - \rho_V)]^{0.25} \tag{23}$$

The dryout region to mist flow (D–M) transition boundary is calculated with the new criterion developed in this study based on the dryout completion data for CO_2:

$$G_M = \left\{\frac{1}{0.502}\left[\ln\left(\frac{0.61}{x}\right) + 0.57\right]\left(\frac{D_{eq}}{\rho_V \sigma}\right)^{-0.16} \left[\frac{1}{g D_{eq} \rho_V (\rho_L - \rho_V)}\right]^{-0.15}\left(\frac{\rho_V}{\rho_L}\right)^{0.09}\left(\frac{q}{q_{crit}}\right)^{-0.72}\right\}^{1.613} \tag{24}$$

which is extracted from the dryout completion (which means the wall remains completely dry) equation developed in this study by solving for G_M from:

$$x_{de} = 0.61 e^{\left[0.57 - 0.502 We_V^{0.16} Fr_{V,Mori}^{0.15} (\rho_V/\rho_L)^{-0.09} (q/q_{crit})^{0.72}\right]} \tag{25}$$

Again, this equation and its dimensionless groups remain the same as those used in the previous method [19] for conventional low reduced pressure refrigerants and only some empirical values were changed when correlating it to the CO_2 data. The vapor Weber number We_V and the vapor Froude number $Fr_{V,Mori}$ are calculated with Eqs. (21) and (22).

The intermittent to bubbly flow (I–B) transition boundary is calculated with the criterion which arises at very high mass velocities and low qualities [12–14]:

$$G_B = \left\{\frac{256 A_{VD} A_{LD}^2 D_{eq}^{1.25} \rho_L (\rho_L - \rho_V) g}{0.3164 (1-x)^{1.75} \pi^2 P_{iD} \mu_L^{0.25}}\right\}^{1/1.75} \tag{26}$$

If $G > G_B$ and $x < x_{IA}$, then the flow is bubbly flow (B).

The following conditions are applied to the transitions in the high vapor quality range:

- If $G_{strat}(x) \geqslant G_{dryout}(x)$, then $G_{dryout}(x) = G_{strat}(x)$
- If $G_{wavy}(x) \geqslant G_{dryout}(x)$, then $G_{dryout}(x) = G_{wavy}(x)$
- If $G_{dryout}(x) \geqslant G_M(x)$, then $G_{dryout}(x) = G_M(x)$

2.2. Comparison of the new flow pattern map for CO_2 to experimental data

Gashe [37] recently conducted an experimental study of CO_2 evaporation inside a 0.8 mm diameter rectangular channel for various mass velocities and observed flow patterns by flow visualization as well. The updated CO_2 flow pattern map was compared to his observations. It should be mentioned here that different names for the same flow

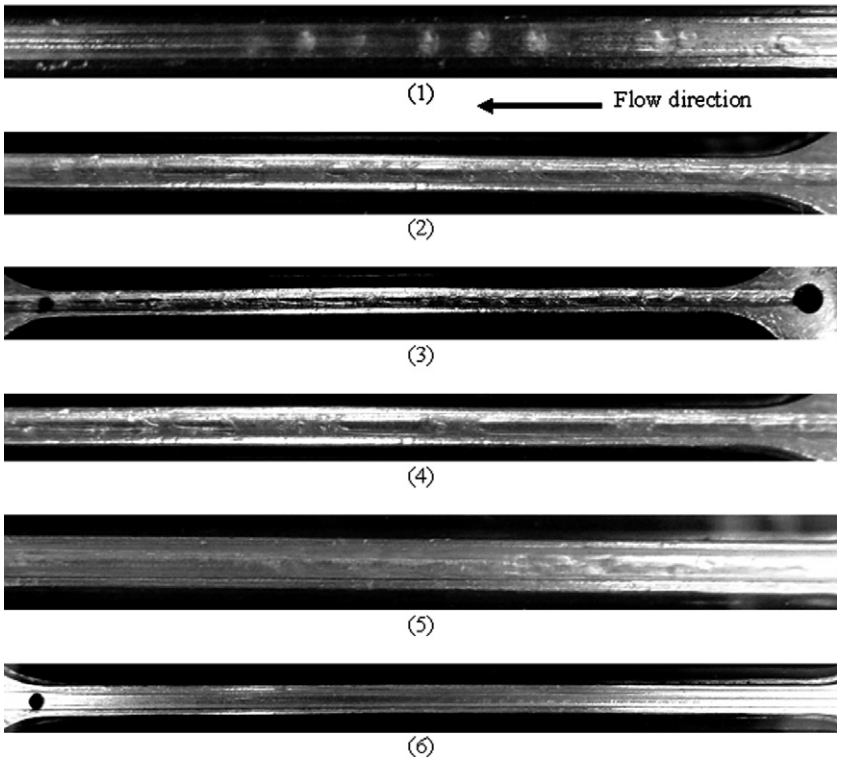

Fig. 2. Flow patterns observed by Gasche [37] at the experimental conditions: $G = 149$ kg/m^2 s, $T_{sat} = 23.3$ °C, $D_{eq} = 0.833$ mm, $q = 1.86$ kW/m^2 where (1), (2), (3) and (4) – plug flow; (5) – slug/annular flow; (6) – annular flow.

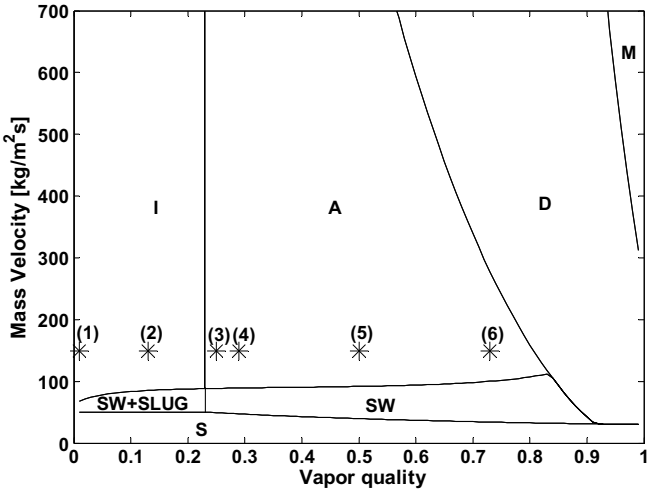

Fig. 3. The experimental data of the observed flow patterns in Fig. 3 shown in the updated CO_2 flow pattern map where (1), (2), (3) and (4) – plug flow; (5) – slug/annular flow; (6) – annular flow.

patterns are used by different authors. Gasche in particular used the definition of plug flow, which is an intermittent flow in our flow pattern map. Just to show one example, Fig. 2 shows the observed flow patterns of CO_2 by Gashe for $D_{eq} = 0.833$ mm (equivalent diameter is used here for the rectangular channel). Fig. 3 shows the observations in Fig. 2 compared to the updated flow pattern map (in the flow pattern map, A is annular flow, D is dryout region, I is intermittent flow, M is mist flow, S is stratified flow and SW is stratified-wavy flow. The stratified to stratified-wavy flow transition is designated as S–SW, the stratified-wavy to intermittent/annular flow transition is designated as SW–I/A, the intermittent to annular flow transition is designated as I–A and so on). It should be mentioned that the observed slug/annular flow of Gashe is counted as an annular flow in the updated flow pattern map. From the photographs in Fig. 2, it seems that the annular flow is the predominant flow in the slug/annular flow defined by Gashe. The observations (3) and (4) are near their correct regimes, especially by the typical flow pattern map standards.

Statistically, 82% of the total 28 flow pattern data of Gashe [37] are identified correctly by the updated flow map, or more specifically, 75% of the intermittent flows and 88% of the annular (slug/annular flow) flows. The updated CO_2 flow pattern map thus predicts the flow patterns observed by Gasche rather well. The lack of other such new data in the literature should justify future experimental studies to obtain more. Furthermore, it is commonly understood that flow pattern transitions do not occur abruptly but over a range of conditions to complete the transition from one stable regime to the other, whereas transition lines on a map only represent the probable "centerline" of this transition range. With the limited data available for CO_2 at this point, predicting the "width" of a transition zone around the transition line is not yet feasible, but it should be a good topic for the future research.

3. CO_2 two-phase pressure drop database and comparison to prediction methods

3.1. Selection of CO_2 two-phase pressure drop data

Five independent experimental studies (1 study is related to macro-scale channel when $D_{eq} > 3$ mm and 4 studies are related to micro-scale channels when $D_{eq} \leqslant 3$ mm) from different laboratories have been selected to form the present database for the two-phase pressure drops of CO_2. Such a distinction between macro- and micro-scale by the threshold diameter of 3 mm is adopted due to the lack of a well-established theory as pointed out by Cheng et al. [1,2] and Thome and Ribatski [11]. The database includes the experimental data of Bredesen et al. [22], Pettersen [26], Pettersen and VestbØstad [31], Zhao et al. [27,28] and Yun and Kim [35,36]. The details of the test conditions covered by the database are summarized in Table 1. The test channels include single circular channels and multi-channels with circular, triangular and rectangular cross-sections and electrical and fluid heated test sections. The data were taken from tables where available or by digitizing the pressure drops from graphs in these publications. All together 387 two-phase pressure drop data points were obtained. Experimental data in some papers were not utilized because: (i) the same data were in more than one paper by the same authors; (ii) some necessary information of the experimental conditions, viz. saturation temperature, vapor quality or tube length was missing; (iii) some data were physically unreasonable such as showing little variation with vapor quality; (iv) the uncertainties of some data were very large; and (vi) some data were only presented in correlated form and could not be extracted. Just one example is mentioned here to be concise. The pressure drop data of Wu et al. [24] have been excluded because their experimental data are 2 times larger than those of R134a at the same test conditions, which is the opposite of the normal trend given by most prediction methods. It must be pointed out here that some authors created confusion because they did not cite if two-phase frictional pressure drops or total two-phase pressure drops (that include the momentum pressure drop in evaporation in a horizontal tube) were being reported, and thus their data cannot be utilized. Consequently, for the reasons noted above, not all the data published are suitable to constitute the present database.

3.2. Comparison of existing two-phase pressure drop models to the database

The empirical two-phase frictional pressure drop methods by Chisholm [3], Friedel [4], Grönnerud [5] and Müller-Steinhagen and Heck [6], a modified Chisholm correlation by Yoon et al. [7] and the flow patterned based pressure drop model by Moreno Quibén and Thome [8–10] were selected for comparison to the two-phase pressure drop database in Table 1. Figs. 4–9 show the comparative results of these two-phase frictional pressure drop methods to the entire CO_2 pressure drop database presented in Table 1. Three criteria were used to analyze the accuracy of the pressure drop prediction methods: the standard deviation, the mean error and the percent of data predicted within ±30%. The statistical analysis of the predicted results is summarized in Table 2. Not one of these models is able to predict the CO_2 two-phase frictional pressure drop data well (note that all have been extrapolated beyond their original conditions to make this comparison for CO_2). The Friedel method gave quite well predictions, but it failed to predict the pressure drop in smaller channels. Therefore, it is necessary to develop a new model for CO_2.

4. Development of a phenomenological two-phase frictional pressure drop model for CO_2

A new two-phase frictional pressure drop model for CO_2 was made here by modifying the model of Moreno Quibén and Thome [8–10] developed for R-22, R-410a and R-134a and incorporating the updated CO_2 flow pattern map, using the CO_2 pressure drop database in Table 1. This is a phenomenological two-phase frictional pressure drop model which is intrinsically related to the flow patterns. Therefore, it is different from the other empirical two-phase pressure drop models tested here. In developing this pressure drop model, two-phase frictional pressure drop data were used. The total pressure drop is the sum of the static pressure drop (gravity pressure drop), the momentum pressure drop (acceleration pressure drop) and the frictional pressure drop:

$$\Delta p_{total} = \Delta p_{static} + \Delta p_m + \Delta p_f \tag{27}$$

For horizontal channels, the static pressure drop equals zero. The momentum pressure drop is calculated as

$$\Delta p_m = G^2 \left\{ \left[\frac{(1-x)^2}{\rho_L(1-\varepsilon)} + \frac{x^2}{\rho_V \varepsilon} \right]_{out} - \left[\frac{(1-x)^2}{\rho_L(1-\varepsilon)} + \frac{x^2}{\rho_V \varepsilon} \right]_{in} \right\} \tag{28}$$

Thus, diabatic experimental tests that measure total pressure drops can be reduced using the above expressions to find the frictional pressure drops.

4.1. Updated frictional pressure drop model based on updated CO_2 flow pattern map

The details of the updated two-phase flow frictional pressure drop model for CO_2 are as follows (For non-circular channels, equivalent diameter D_{eq} is used in the pressure drop model to keep consistent with that in the flow pattern map. Using equivalent diameter gives the same mass velocity as in the non-circular channel and thus correctly reflects the mean liquid and vapor velocities, something using hydraulic diameter in a two-phase flow does. For circular channels, equivalent diameter D_{eq} equals hydraulic

Table 1
Database of CO_2 pressure drops in evaporation

Data source	Channel configuration and material	Equivalent diameter D_{eq} (mm)	Saturation temperature T_{sat} (°C)	Reduced pressure p_r	Mass flux G (kg/m^2 s)	Heat flux q (kW/m^2)	Data points	Heating method
Bredesen et al. [22]	Single circular tube, stainless steel	7	−25	0.21	200, 300, 400	3, 6, 9	319	Electrical heating
			−10	0.37				
			5	0.54				
Pettersen [26]	Multi-channel with 25 circular channels, aluminium	0.8	0	0.47	190, 280, 380,	10	24	Heated by water
			10	0.61				
			20	0.78				
Pettersen and Vestbøstad [31]	Multi-channel with 25 circular channels, aluminium	0.8	0	0.47	200, 300, 400,	10	20	Heated by water
			10	0.61				
			20	0.78				
Zhao et al. [27,28]	Multi-triangular channels, stainless steel	1.15 (0.86)[a]	10	0.61	300	11	9	Electrical heating
Yun and Kim [35,36]	Multi-rectangular channels	1.74 (1.53)[a]	5	0.54	200, 300, 400	15	15	Electrical heating

[a] The value in the bracket is hydraulic diameter (D_h), for non-circular channels, equivalent diameter is used. For circular channels, equivalent diameters equal hydraulic diameters.

diameter D_h, to make it clear, equivalent diameter D_{eq} is used in the following equations.):

(1) CO_2 frictional pressure drop model for annular flow (A): The basic equation is the same as that of the Moreno Quibén and Thome [8–10] pressure drop model:

$$\Delta p_A = 4 f_A \frac{L}{D_{eq}} \frac{\rho_V u_V^2}{2} \tag{29}$$

where the two-phase flow friction factor of annular flow f_A was correlated according CO_2 experimental data here (considering the main parameters which affect the two-phase pressure drops for CO_2) as:

$$f_A = 3.128 Re_V^{-0.454} We_L^{-0.0308} \tag{30}$$

This correlation is thus different from that of the Moreno Quibén and Thome [8–10] pressure drop model. The mean velocity of the vapor phase u_V is calculated as

$$u_V = \frac{Gx}{\rho_V \varepsilon} \tag{31}$$

The void fraction ε is calculated using Eq. (8). The vapor phase Reynolds number Re_V and the liquid phase Weber number We_L based on the mean liquid phase velocity u_L are calculated as

$$Re_V = \frac{GxD_{eq}}{\mu_V \varepsilon} \tag{32}$$

$$We_L = \frac{\rho_L u_L^2 D_{eq}}{\sigma} \tag{33}$$

$$u_L = \frac{G(1-x)}{\rho_L (1-\varepsilon)} \tag{34}$$

(2) CO_2 frictional pressure drop model for slug and intermittent flow (Slug + I): A proration is proposed to avoid any jump in the pressure drops between these two flow patterns, so that the Moreno Quibén and Thome [8–10] pressure drop model is updated to become:

$$\Delta p_{SLUG+I} = \Delta p_{LO}\left(1 - \frac{\varepsilon}{\varepsilon_{IA}}\right) + \Delta p_A \left(\frac{\varepsilon}{\varepsilon_{IA}}\right) \tag{35}$$

where Δp_A is calculated with Eq. (29) and the single-phase frictional pressure drop considering the total vapor–liquid two-phase flow as liquid flow Δp_{LO} is calculated as

$$\Delta p_{LO} = 4 f_{LO} \frac{L}{D_{eq}} \frac{G^2}{2\rho_L} \tag{36}$$

The friction factor is calculated with the Blasius equation as

$$f_{LO} = \frac{0.079}{Re_{LO}^{0.25}} \tag{37}$$

where Reynolds number Re_{LO} is calculated as

$$Re_{LO} = \frac{GD_{eq}}{\mu_L} \tag{38}$$

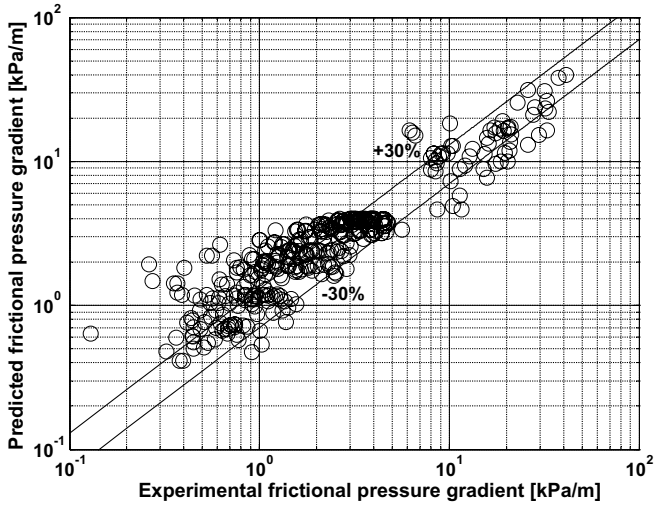

Fig. 4. Comparison of the predicted two-phase frictional pressure gradients by the Chisholm method [3] to the entire database (56.1% of the data are predicted within ±30%).

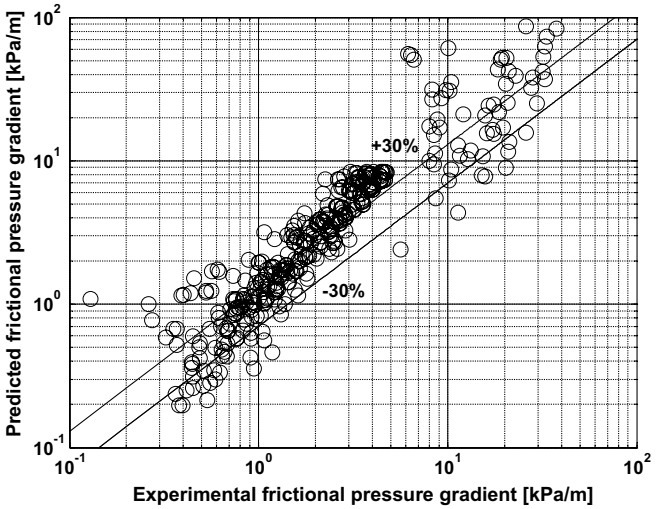

Fig. 6. Comparison of the predicted two-phase frictional pressure gradients by the Grönnerud method [5] to the entire database (30.2% of the data are predicted within ±30%).

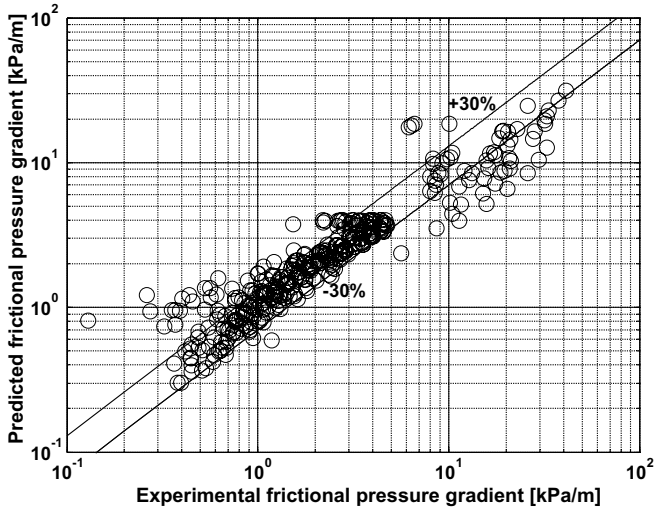

Fig. 5. Comparison of the predicted two-phase frictional pressure gradients by the Friedel method [4] to the entire database (71.1% of the data are predicted within ±30%).

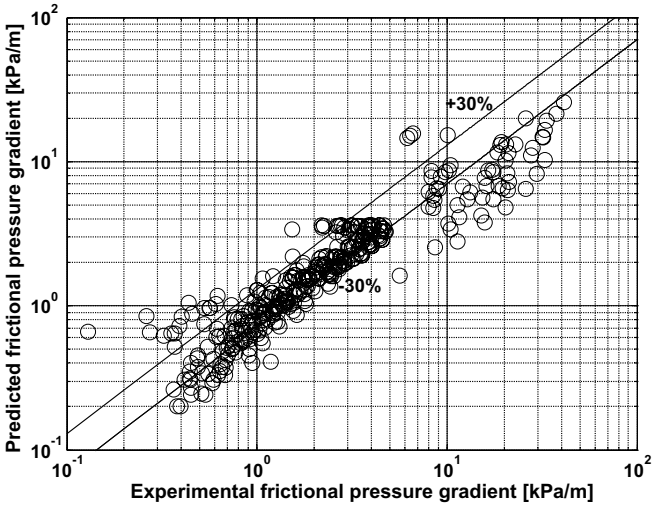

Fig. 7. Comparison of the predicted two-phase frictional pressure gradients by the Müller-Steinhagen and Heck method [6] to the entire database (55.8% of the data are predicted within ±30%).

(3) CO_2 frictional pressure drop model for stratified-wavy flow (SW): The equation is kept the same as that of the Moreno Quibén and Thome [8–10] pressure drop model:

$$\Delta p_{SW} = 4 f_{SW} \frac{L}{D_{eq}} \frac{\rho_V u_V^2}{2} \tag{39}$$

where the two-phase friction factor of stratified-wavy flow f_{SW} is calculated with the following interpolating expression (a modification of that used in the Moreno Quibén and Thome [8–10] pressure drop model) based on the CO_2 database:

$$f_{SW} = {\theta^*_{dry}}^{0.02} f_V + \left(1 - \theta^*_{dry}\right)^{0.02} f_A \tag{40}$$

and the dimensionless dry angle θ^*_{dry} is defined as

$$\theta^*_{dry} = \frac{\theta_{dry}}{2\pi} \tag{41}$$

where θ_{dry} is the dry angle as shown in Fig. 1. The dry angle θ_{dry} defines the flow structure and the ratio of the tube perimeter in contact with vapor. For the stratified-wavy regime (SW), the following equation is proposed:

$$\theta_{dry} = \theta_{strat} \left(\frac{G_{wavy} - G}{G_{wavy} - G_{strat}} \right)^{0.61} \tag{42}$$

The single-phase friction factor of the vapor phase f_V is calculated as

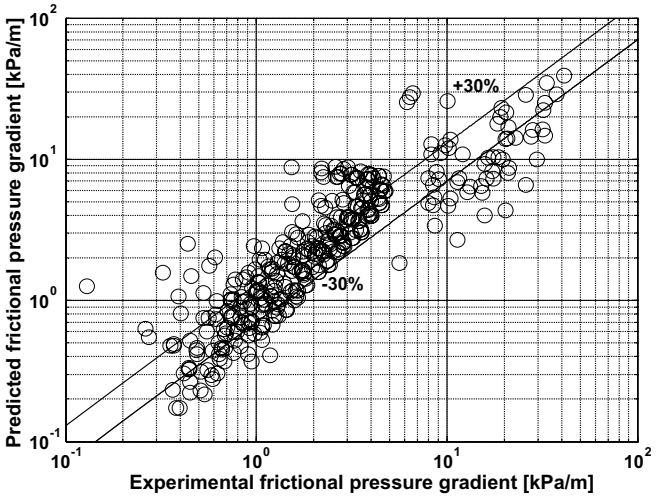

Fig. 8. Comparison of the predicted two-phase frictional pressure gradients by the modified Chisholm method by Yoon et al. [7] to the entire database (47% of the data are predicted within ±30%).

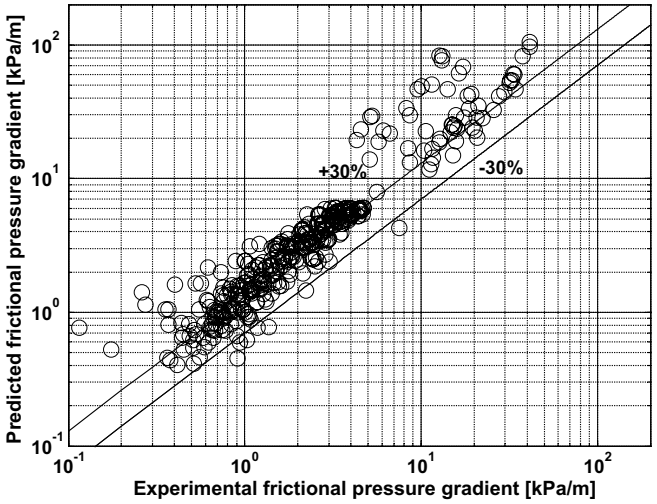

Fig. 9. Comparison of the predicted two-phase flow frictional pressure gradients by the Moreno Quibén and Thome model [8–10] to the entire database (42.4% of the data are predicted within ±30%).

$$f_V = \frac{0.079}{Re_V^{0.25}} \tag{43}$$

where the vapor Reynolds number is calculated with Eq. (32).

(4) CO_2 frictional pressure drop model for slug-stratified wavy flow (Slug + SW): It is proposed to avoid any jump in the pressure drops between these two flow patterns and to updated the Moreno Quibén and Thome [8–10] pressure drop model as

$$\Delta p_{SLUG+SW} = \Delta p_{LO}\left(1 - \frac{\varepsilon}{\varepsilon_{IA}}\right) + \Delta p_{SW}\left(\frac{\varepsilon}{\varepsilon_{IA}}\right) \tag{44}$$

where Δp_{LO} and Δp_{SW} are calculated with Eqs. (36) and (39), respectively.

(5) CO_2 frictional pressure drop model for mist flow (M): The following expression is kept the same as that in the Moreno Quibén and Thome [8–10] pressure drop model:

$$\Delta p_M = 4 f_M \frac{L}{D_{eq}} \frac{G^2}{2\rho_H} \tag{45}$$

The homogenous density ρ_H is defined as

$$\rho_H = \rho_L(1 - \varepsilon_H) + \rho_V \varepsilon_H \tag{46}$$

where the homogenous void fraction ε_H is calculated as

$$\varepsilon_H = \left(1 + \frac{(1-x)}{x}\frac{\rho_V}{\rho_L}\right)^{-1} \tag{47}$$

and the friction factor of mist flow f_M was correlated according to the CO_2 experimental data, which is different from that in the Moreno Quibén and Thome [8–10] pressure drop model, as

$$f_M = \frac{91.2}{Re_M^{0.832}} \tag{48}$$

The Reynolds number is defined as

$$Re_M = \frac{G D_{eq}}{\mu_H} \tag{49}$$

where the homogenous dynamic viscosity is calculated as proposed by Ciccitti et al. [44]:

$$\mu_H = \mu_L(1 - x) + \mu_V x \tag{50}$$

The constants in Eq. (48) are quite different from those in the Blasius equation. The reason is possibly because there are limited experimental data in mist flow in the data-

Table 2
Statistical analysis of the two-phase frictional pressure drop predictions for all data points

Models and data used for comparison	Data points	Percentage of predicted points within ±30%	Mean error $\lvert\bar{\xi}\rvert$	Standard deviation σ
Chisholm model [3]	387	56.1%	48.6%	73.8%
Friedel model [4]	387	71.1%	30.9%	55.8%
Grönnerud model [5]	387	30.2%	75%	113.1%
Müller-Steinhagen and Heck model [6]	387	55.8%	33.3%	44.3%
Modified Chisholm by Yoon et al. model [7]	387	47%	34.7%	93.7%
Moreno Quibén and Thome model [8–10]	387	42.4%	50.1%	90.6%
New model	387	74.7%	28.6%	44.3%

$\sigma = \sqrt{\frac{1}{N}\sum_{i=1}^{N}(\xi_i - \bar{\xi})^2}$; $\lvert\bar{\xi}\rvert = \frac{1}{N}\sum_{i=1}^{N}\lvert\xi_i\rvert$; $\xi_i = \frac{\text{Predicted}-\text{Measured}}{\text{Measured}}$.

base and also perhaps a lower accuracy of these experimental data. Therefore, more accurate experimental data are needed in mist flow to further verify this correlation or modify it if necessary in the future.

(6) CO_2 frictional pressure drop model for dryout region (D): The linear interpolating expression is kept the same as that in the Moreno Quibén–Thome pressure drop model as

$$\Delta p_{\text{dryout}} = \Delta p_{\text{tp}}(x_{\text{di}}) - \frac{x - x_{\text{di}}}{x_{\text{de}} - x_{\text{di}}}\left[\Delta p_{\text{tp}}(x_{\text{di}}) - \Delta p_{\text{M}}(x_{\text{de}})\right] \quad (51)$$

where $\Delta p_{\text{tp}}(x_{\text{di}})$ is the frictional pressure drop at the dryout inception quality x_{di} and is calculated with Eq. (29) for annular flow or with Eq. (39) for stratified-wavy flow, and $\Delta p_{\text{M}}(x_{\text{de}})$ is the frictional pressure drop at the completion quality x_{de} and is calculated with Eq. (45). x_{di} and x_{de} are, respectively, calculated with Eqs. (20) and (25).

(7) CO_2 frictional pressure drop model for stratified flow (S): No data fell into this flow regime but for completeness, the method is kept the same as that in the Moreno Quibén and Thome [8–10] pressure drop model as

For $x \geqslant x_{\text{IA}}$:

$$\Delta p_{\text{strat}(x \geqslant x_{\text{IA}})} = 4 f_{\text{strat}(x \geqslant x_{\text{IA}})} \frac{L}{D_{\text{eq}}} \frac{\rho_{\text{V}} u_{\text{V}}^2}{2} \quad (52)$$

where the mean velocity of the vapor phase u_{V} is calculated with Eq. (31) and the two-phase friction factor of stratified flow $f_{\text{strat}(x \geqslant x_{\text{IA}})}$ is calculated as

$$f_{\text{strat}(x \geqslant x_{\text{IA}})} = \theta^*_{\text{strat}} f_{\text{V}} + \left(1 - \theta^*_{\text{strat}}\right) f_{\text{A}} \quad (53)$$

The single-phase friction factor of the vapor phase f_{V} and the two-phase friction factor of annular flow f_{A} are calculated with Eqs. (43) and (30), respectively, and the dimensionless stratified angle θ^*_{strat} is defined as

$$\theta^*_{\text{strat}} = \frac{\theta_{\text{strat}}}{2\pi} \quad (54)$$

where the stratified angle θ_{strat} is calculated with Eq. (13).

For $x < x_{\text{IA}}$:

$$\Delta p_{\text{strat}(x < x_{\text{IA}})} = \Delta p_{\text{LO}}\left(1 - \frac{\varepsilon}{\varepsilon_{\text{IA}}}\right) + \Delta p_{\text{strat}(x \geqslant x_{\text{IA}})}\left(\frac{\varepsilon}{\varepsilon_{\text{IA}}}\right) \quad (55)$$

where Δp_{LO} and $\Delta p_{\text{strat}(x \geqslant x_{\text{IA}}IA)}$ are calculated with Eqs. (36) and (52), respectively.

(8) CO_2 frictional pressure drop model for bubbly flow (B): No data are available for this regime but keeping consistent with the frictional pressure drops in the neighboring regimes and following the same format as the others without creating a jump at the transition (there is no such a model in the Moreno Quibén and Thome [8–10] pressure drop model), the following expression is used:

$$\Delta p_{\text{B}} = \Delta p_{\text{LO}}\left(1 - \frac{\varepsilon}{\varepsilon_{\text{IA}}}\right) + \Delta p_{\text{A}}\left(\frac{\varepsilon}{\varepsilon_{\text{IA}}}\right) \quad (56)$$

where Δp_{LO} and Δp_{A} are calculated with Eqs. (36) and (29), respectively. Further experimental data are needed to verify or modify this model.

4.2. Comparisons of the updated pressure drop model to the database

The new updated CO_2 two-phase frictional pressure drop model was compared to the CO_2 two-phase pressure drop database in Table 1. Fig. 10a shows the comparison of the new pressure drop model to the experimental data of Bredesen et al. [22] at the indicated experimental conditions and Fig. 10b shows the corresponding flow pattern map at the same experimental condition as that in Fig. 10a. The new model predicts the experimental data very well. Fig. 11 shows the comparative results of the predictions by the new CO_2 pressure drop model to the entire two-phase pressure drop database in Table 1. In addition, the statistical results of the predicted and experimental data for individual research according to the percent of data predicted within ±30% are presented in Fig. 11.

The statistical analysis of the comparison of the leading methods and the new model to the entire database is sum-

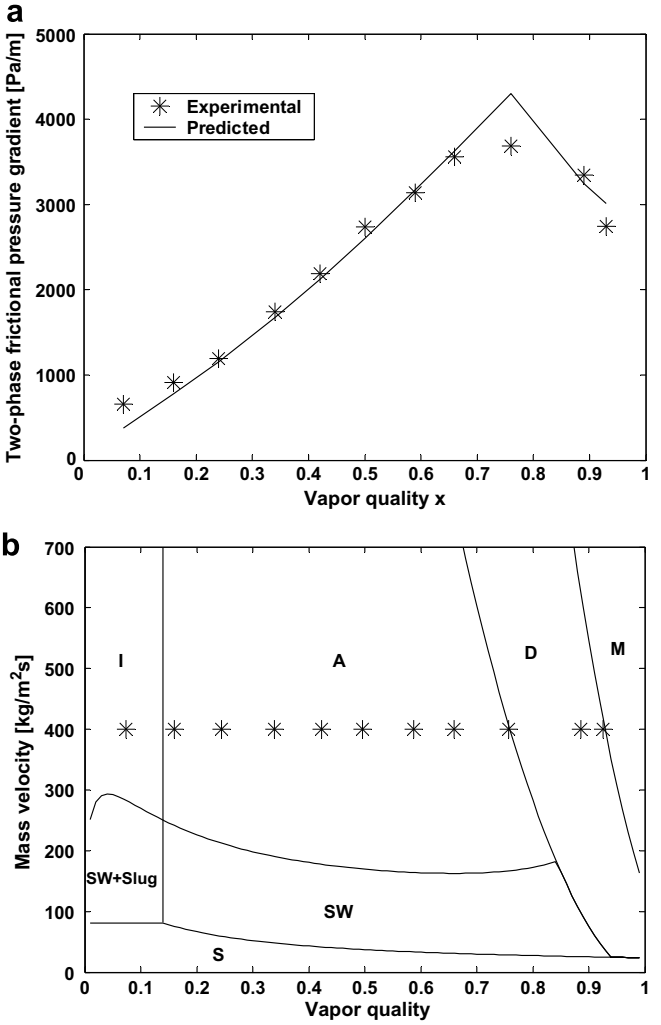

Fig. 10. (a) Comparison of the new CO_2 pressure drop model to the experimental data of Bredesen et al. [22] at the experimental conditions: $G = 400$ kg/m^2 s, $T_{\text{sat}} = -10$ °C, $D_{\text{eq}} = 7$ mm and $q = 9$ kW/m^2; (b) The corresponding flow pattern map at the same experimental condition as in (a).

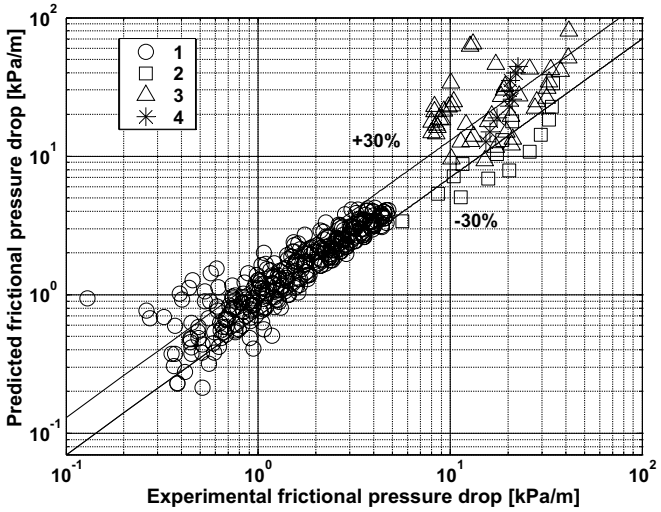

Fig. 11. Comparison of the predicted frictional pressure gradients by the new model to the entire database (74.7% of the data are predicted within ±30%). By individual study, the following percent of data are captured with ±30%: (1) – Bredesen et al. [22] 81.5%, (2) –Yun and Kim [35,36] 33.3%, (3) – Pettersen [26] and Pettersen and VestbØstad [31] 43.2%, and (4) – Zhao et al. [27,28] 55.6% (Note that 2, 3 and 4 are the data of smaller channels).

marized in Table 2. As shown in Table 2, the new CO_2 two-phase frictional pressure drop model predicts the CO_2 pressure drop data better than other existing empirical methods. However, the new model is only a slightly better than the Friedel method. To further compare the Friedel method and the new model, analysis has been done according to the predicted results for macro-scale channel pressure drop data (the data of Bredesen et al. [22] as indicated in Table 1) and for the micro-scale channel pressure drop data (the data of Pettersen [26] and Pettersen and VestbØstad [31], the data of Zhao et al. [27,28] and the data of Yun and Kim [35,36] as indicated in Table 1). The new model predicts 81.5% of the macro-scale channel pressure drop data with ±30% whereas the Friedel method predicts 77% of the macro-scale channel data with ±30%. However, the new model has smaller a standard deviation and mean error. Furthermore, it is better than the Friedel method for the prediction of the macro-scale channel data. As for micro-scale channel data, the new model predicts 44% of the micro-scale channel pressure drop data with ±30% while the Friedel method predicts only 35% of the micro-scale channel pressure drop data with ±30%. However, neither method is good enough for the prediction of micro-scale channel pressure drop data, possibly because there are very limited experimental data points and it is more difficult to measure such data in micro-scale channels without disturbing the flow itself. For instance, the experimental data sets have a level of scatter up to 50% in the micro-scale channels here. Therefore, more accurate experimental data for a wide of conditions (especially at high vapor qualities and in micro-scale channels) are needed to further improve the model.

In addition, the detailed breakdown of the statistical analysis for the new pressure drop model is summarized in Table 3. Most of the experimental data points (75.5%) are in annular flow and 75.7% of experimental data in annular flow are predicted within ±30%. However, the predictions in some regions such as S-Slug and SW are not satisfactory. Generally, the new pressure drop model reasonably predicts the database and importantly captures the trends in the data too. Nonetheless, there are not many experimental data available covering some flow patterns as can be seen in Table 3 and future experimental work is recommended to address these conditions.

5. Conclusions

An updated flow pattern map was developed for CO_2 to extend the previous Cheng–Ribatski–Wojtan–Thome CO_2 flow pattern map [1,2] to a wider range of conditions. The updated map was compared to the new flow pattern observations for CO_2 available in the literature and good agreement was obtained. The updated map is applicable to a wider range of conditions: tube diameters from 0.6 to 10 mm, mass velocities from 50 to 1500 kg/m^2 s, heat fluxes from 1.8 to 46 kW/m^2 and saturation temperatures from −28 to +25 °C (reduced pressures from 0.21 to 0.87).

A CO_2 two-phase pressure drop database was set up and compared to the leading empirical pressure drop methods: the correlations by Chisholm [3], Friedel [4], Grönnerud [5] and Müller-Steinhagen and Heck [6], a modified Chisholm correlation by Yoon et al. [7] and the flow pattern based model of Moreno Quibén and Thome [8–10]. None of these models was able to predict the CO_2 pressure drop data well. Therefore, a new flow pattern based phenomenological model of two-phase frictional pressure drop for CO_2

Table 3
Statistical analysis of new frictional pressure drop model by flow patterns

Flow pattern	Percentage of predicted points within ±30%	Predicted data points	Number of data points within regime	Flow pattern data percentage
S-SLUG	0%	0	2	0.52%
I-SLUG	83.3%	5	6	1.55%
SW	58.3%	7	12	3.1%
Annular	75.7%	221	292	75.5%
Dryout	74.6%	50	67	17.3%
Mist flow	75%	6	8	2.07%
Total	74.7%	289	387	100%

was developed. The new CO_2 two-phase flow pressure drop model predicts the CO_2 pressure drop database better than the existing methods. Although the new model is a slightly better than the Friedel method for the prediction of the entire database, it is much better than the Friedel for the prediction of micro-scale channel data. However, due to the very few and less accurate experimental data in micro-scale channels currently available, the new CO_2 pressure drop model does not predict these data satisfactorily. It is suggested that additional, more accurate experimental CO_2 pressure drop data be obtained to further test or improve the model in the future.

Acknowledgements

The Laboratory of Heat and Mass Transfer (LTCM) at École Polytechnique Fédérale de Lausanne (EPFL) wishes to thank Valeo Engine Cooling in France for its financial and technical support on this CO_2 heat transfer and flow project. The constructive discussion and suggestions with Mr. Lorenzo Consolini of LTCM in the development of the CO_2 two-phase frictional pressure drop model are greatly appreciated. The authors wish to thank Prof. Gasche of the Universidade Estadual Paulista (UNESP) in Brazil for providing his experimental flow pattern data and photographs.

References

[1] L. Cheng, G. Ribatski, L. Wojtan, J.R. Thome, New flow boiling heat transfer model and flow pattern map for carbon dioxide evaporating inside tubes, Int. J. Heat Mass Transfer 49 (2006) 4082–4094.

[2] L. Cheng, G. Ribatski, L. Wojtan, J.R. Thome, Erratum to: New flow boiling heat transfer model and flow pattern map for carbon dioxide evaporating inside tubes [Heat Mass Transfer 49 (21–22) (2006) 4082–4094], Int. J. Heat Mass Transfer 50 (2007) 391.

[3] D. Chisholm, Pressure gradients due to friction during the flow of evaporating two-phase mixtures in smooth tubes and channels, Int. J. Heat Mass Transfer 16 (1973) 347–358.

[4] L. Friedel, Improved friction drop correlations for horizontal and vertical two-phase pipe flow, in: European Two-phase Flow Group Meeting, Ispra, Italy, 1979, paper E2.

[5] R. Grönnerud, Investigation of liquid hold-up, flow-resistance and heat transfer in circulation type of evaporators. Part IV: Two-phase flow resistance in boiling refrigerants, in: Annexe 1972-1, Bull. De l'Inst. Du Froid, 1979.

[6] H. Müller-Steinhagen, K. Heck, A simple friction pressure drop correlation for two-phase flow in pipes, Chem. Eng. Process 20 (1986) 297–308.

[7] S.H. Yoon, E.S. Cho, Y.W. Hwang, M.S. Kim, K. Min, Y. Kim, Characteristics of evaporative heat transfer and pressure drop of carbon dioxide and correlation development, Int. J. Refrig. 27 (2004) 111–119.

[8] J. Moreno Quibén, J.R. Thome, Flow pattern based two-phase frictional pressure drop model for horizontal tubes. Part I: Diabatic and adiabatic experimental study, Int. J. Heat Fluid Flow (2007), doi:10.1016/j.ijheatfluidflow.2007.01.003.

[9] J. Moreno Quibén, J.R. Thome, Flow pattern based two-phase frictional pressure drop model for horizontal tubes. Part II: New phenomenological model, Int. J. Heat Fluid Flow (2007), doi:10.1016/j.ijheatfluidflow.2007.01.004.

[10] J. Moreno Quibén, Experimental and analytical study of two-phase pressure drops during evaporation in horizontal tubes, Ph.D. Thesis, Swiss Federal Institute of Technology (EPFL), Lausanne, Switzerland, 2005.

[11] J.R. Thome, G. Ribatski, State-of-the art of flow boiling and two-phase flow of CO_2 in macro- and micro-channels, Int. J. Refrig. 28 (2006) 1149–1168.

[12] N. Kattan, J.R. Thome, D. Favrat, Flow boiling in horizontal tubes. Part 1: Development of a diabatic two-phase flow pattern map, J. Heat Transfer 120 (1998) 140–147.

[13] N. Kattan, J.R. Thome, D. Favrat, Flow boiling in horizontal tubes: Part 2-new heat transfer data for five refrigerants, J. Heat Transfer 120 (1998) 148–155.

[14] N. Kattan, J.R. Thome, D. Favrat, Flow boiling in horizontal tubes: Part-3: Development of a new heat transfer model based on flow patterns, J. Heat Transfer 120 (1998) 156–165.

[15] O. Baker, Design of pipe lines for simultaneous flow of oil and gas, Oil Gas J. 53 (1954) 185–190.

[16] Y. Taitel, A.E. Dukler, A model for predicting flow regime transitions in horizontal and near horizontal gas–liquid flow, AIChE J. 22 (1976) 47–55.

[17] K. Hashitume, Flow pattern and void fraction of refrigerant two-phase flow in a horizontal pipe, Bull. JSME 26 (1983) 1597–1602.

[18] D. Steiner, VDI-Wärmeatlas, Verein Deutscher Ingenieure VDI-Gessellschaft Verfahrenstechnik und Chemieingenieurwessen (GCV), Düsseldorf, Ch. Hbb, 1993.

[19] L. Wojtan, T. Ursenbacher, J.R. Thome, Investigation of flow boiling in horizontal tubes: Part I – A new diabatic two-phase flow pattern map, Int. J. Heat Mass Transfer 48 (2005) 2955–2969.

[20] L. Wojtan, T. Ursenbacher, J.R. Thome, Investigation of flow boiling in horizontal tubes: Part II – Development of a new heat transfer model for stratified-wawy, dryout and mist flow regimes, Int. J. Heat Mass Transfer 48 (2005) 2970–2985.

[21] M.B. Ould-Didi, N. Kattan, J.R. Thome, Prediction of two-phase pressure gradients of refrigerants in horizontal tubes, Int. J. Refrig. 25 (2002) 935–947.

[22] A. Bredesen, A. Hafner, J. Pettersen, P. Neksa, K. Aflekt, Heat transfer and pressure drop for in-tube evaporation of CO_2, in: Proceedings of the International Conference on Heat Transfer Issues in Natural Refrigerants, University of Maryland, USA, 1997, pp. 1–15.

[23] A. Bredesen, K. Aflekt, J. Pettersen, A. Hafner, P. Neksa, G. Skaugen, Studies on CO_2 heat exchangers and heat transfer, in: Workshop Proceedings – CO_2 Technologies in Refrigeration, Heat Pumps and Air Conditioning Systems, Trondheim, Norway, 1997, pp. 329-358.

[24] X.M. Wu, H.Y. Zhao, W.C. Wang, L. Jing, L. Zhang, Experimental study on evaporating heat transfer of CO_2 in thin tube, J. Eng. Thermophys. (Gong Cheng Re Wu Li Xue Bao) 26 (2005) 823–825.

[25] S.H. Yoon, E.S. Cho, M.S. Kim, Y. Kim, Studies on the evaporative heat transfer and pressure drop of carbon dioxide near the critical point, in: 21st IIR International Congress of Refrigeration, Washington DC, USA, 2003, paper ICR0477.

[26] J. Pettersen, Flow vaporization of CO_2 in microchannel tubes, Exp. Therm. Fluid Sci. 28 (2004) 111–121.

[27] Y. Zhao, M. Molki, M.M. Ohadi, S.V. Dessiatoun, Flow boiling of CO_2 in microchannels, ASHRAE Trans. 106 (Part I) (2000) 437–445.

[28] Y. Zhao, M. Molki, M.M. Ohadi, Heat transfer and pressure drop of CO_2 flow boiling in microchannels, in: Proceedings of the ASME Heat Transfer Division, Vol. 2, 2000, pp. 243–249.

[29] S. Jeong, E. Cho, H. Kim, Evaporative heat transfer and pressure drop of in a microchannel tube, in: Proceedings of the third International Conference on Microchannels and minichannels, 2005, Toronto, Ontario, Canada, Part B, pp. 103–108.

[30] P. Neksa, J. Pettersen, G. Skaugen, Heat transfer and pressure drop of evaporating CO_2 in microchannels and system design implications of critical heat flux conditions, in: Proceedings of 2001 ASME International Mechanical Engineering Congress and Exposition, AES, vol. 41, New York, NY, 2001, pp. 261–268.

[31] J. Pettersen, K. VestbØstad, Heat transfer and pressure drop for flow of supercritical and subcritical in microchannel tubes, in: Workshop Proceedings-Selected Issue on CO_2 as Working Fluid in Compression System, Trondheim, Norway, 2000, pp. 101–114.
[32] J. Pettersen, Two-phase flow pattern, heat transfer and pressure drop in microchannel vaporization of CO_2, ASHRAE Trans. (2003) 523–532.
[33] J. Pettersen, R. Rieberer, S.T. Munkejord, Heat transfer and pressure drop characteristics of evaporating carbon dioxide in microchannel tubes, in: Proceedings of fourth IRR-Gustav Lorenzen Conference on Natural Working Fluid, Purdue University, USA, 2000, pp. 107–114.
[34] J. Pettersen, Heat transfer and pressure drop characteristics of evaporating carbon dioxide in microchannel tubes. in: Natural working fluids, Proceedings of the 4th IIR-Gustav Lorentzen Conference on Natural Working Fluids, Purdue University, USA, 2000, pp. 324–334.
[35] R. Yun, Y. Kim, Two-phase pressure drop of CO_2 in mini tubes and microchannels, in: First International Conference on Microchannels and Minichannels, Rochester, NY, 2003, pp. 507–511.
[36] R. Yun, Y. Kim, Two-phase pressure drop of CO_2 in mini tubes and microchannels, Microscale Therm. Eng. 8 (2004) 259–270.
[37] J.L. Gasche, Carbon doxide evaporation in a single micro-channel, J. Brazil Soc. Mech. Sci. Eng. 28 (1) (2006) 69–83.
[38] REFPROP. NIST Refrigerant Properties Database 23, Gaithersburg, MD, 1998, Version 6.01.
[39] J.R. Thome, J. El Hajal, Two-phase flow pattern map for evaporation in horizontal tubes: Latest version, in: first International Conference on Heat Transfer, Fluid Mechanics and Thermodynamics, Kruger Park, South Africa, 8–10 April, 2002, pp. 182–188.
[40] Z. Rouhani, E. Axelsson, Calculation of volume void fraction in a subcooled and quality region, Int. J. Heat Mass Transfer 17 (1970) 383–393.
[41] D. Biberg, An explicit approximation for the wetted angle in two-phase stratified pipe flow, Can. J. Chem. Eng. 77 (1999) 1221–1224.
[42] H. Mori, S. Yoshida, K. Ohishi, Y. Kokimoto, Dryout quality and post dryout heat transfer coefficient in horizontal evaporator tubes, in: Proceedings of the 3rd European Thermal Sciences Conference, 2000, pp. 839–844.
[43] S.S. Kutateladze, On the transition to film boiling under natural convection, Kotloturbostroenie (3) (1948) 10–12.
[44] A. Ciccitti, C. Lombardi, M. Silvestri, G. Soldaini, R. Zavattarelli, Two-phase cooling experiments—pressure drop, heat transfer and burnout measurements, Energia Nucleare 7 (6) (1960) 407–425.